



# Probing energy transfer mechanism via the upconversion spectra of $Tm^{3+}/Yb^{3+}:LiNbO_3$ by tri-doping with $Ba^{2+}$ in different site occupations

Zhihua Liu <sup>b</sup>, Yunzhong Zhu <sup>a,\*</sup>, Wenjia Wang <sup>b</sup>, Decai Ma <sup>a</sup>, Biao Wang <sup>a,\*\*</sup>

<sup>a</sup> Sino French Institute of Nuclear Engineering and Technology, Sun Yat-sen University, Zhuhai, 519082, China

<sup>b</sup> School of Physics, Sun Yat-sen University, Guangzhou, 510275, China



## ARTICLE INFO

### Article history:

Received 28 September 2019

Received in revised form

21 January 2020

Accepted 21 January 2020

Available online 24 January 2020

### Keywords:

Energy transfer mechanism

Lithium niobate

Blue upconversion emission

## ABSTRACT

Metal doping has been an efficient method to enhance upconversion (UC) luminescence, however, the relationship between fluorescence kinetics and site occupation of luminescence center has barely been revealed. To solve this issue, we have designed a tri-doping system of various  $Ba^{2+}$  doped  $Tm^{3+}/Yb^{3+}:LiNbO_3$  to investigate the energy transfer (ET) rate and the site occupation quantitatively, where 4.8 and 7.9 folds enhancement of blue and red emission has been achieved, respectively. Owing to the sensitive 4f-4f transition between lanthanide ions, the ion environment could be presented vividly by the zigzag-shaped UC intensity variation for different  $Ba^{2+}$  doping concentrations. Then, the corresponding ET rate equations are established by steady-state rate equations which draw the site occupation process of lanthanide ions simultaneously. The calculated results for Föster ET rate, local optical power density, and pump power absorption illustrate that  $Ba^{2+}$  could adjust the ET rate by transforming the site of lanthanide ions in crystal lattice. More importantly, this method could shed light on the mechanism of UC enhancement by modulating ET rate via ion doping.

© 2020 Elsevier B.V. All rights reserved.

## 1. Introduction

Frequency conversion of photon is one of the most attractive researches to achieve full-wave band radiation. As the main stream of frequency conversion, UC emission is a typical anti-Stokes process in which one-off emission following by continuously photon absorption via a long-lived 4f electronic state of lanthanide ions [1–3]. Upconversion process could transfer infrared light into visible light and enlarge the optical spectra response range of devices, which has great applications for solar cell, bioluminescence, temperature sensor, laser, solid-state lighting and display technologies [3–11]. Lanthanide doped particles are the most familiar UC materials [12,13] for the great monochromaticity, but further applications are limited by their low conversion efficiency. Thus, methods such as ion doping, concentration optimization, core-shell construction and plasmonic enhancement [14–17] are used to

enhance UC intensity. Metal doping ( $Li^+$  [14],  $Zn^{2+}$  [18] and  $Mn^{2+}$  [19–21]) has been proved an efficient approach to increase UC luminescence via tailoring the local crystal field of host lattice, namely, modifying the ion environment of lanthanide ions. Since the ion distance between the lanthanides determines the ET rate, the site occupation of lanthanide ions has a close connection with UC mechanism. However, as a major factor to modulate ET rate in multiple-doped system, the specific site occupation of lanthanide ions is still undecipherable.

To investigate the site occupation of lanthanide ions, we have designed a metal-doped system whose UC spectra and steady state rate equations are associated with UV–Vis and Raman measurements. The widely investigated congruent lithium niobate (CLN) is taken as the study carrier for its well-informed topic of great influence in the fields of optical and photoelectric devices [22–25]. Moreover, the stable physico-chemical property and low cut-off phonon energy (among oxides) make CLN a suitable matrix for UC luminescence [26]. In addition, CLN has different kinds of defects like oxygen vacancy, anti-site niobium and lithium vacancy, which creates enough room for dopants [27,28]. Among lanthanide ions,  $Tm^{3+}$  is the best candidate for converting infrared light into visible blue light [29,30]. Because the mono-doped  $Tm^{3+}$  material

\* Corresponding author.

\*\* Corresponding author.

E-mail addresses: zhuyz7@mail.sysu.edu.cn (Y. Zhu), wangbiao@mail.sysu.edu.cn (B. Wang).

exhibits low absorption cross section for 980 nm pump power, Yb<sup>3+</sup> should be co-doped as a sensitizer to enhance 980 nm absorption for its unique energy levels [31,32]. In addition, different concentrations of Ba<sup>2+</sup> are tri-doped to modify the site occupation of above lanthanide ions. The corresponding UC process is described quantitatively via the steady state rate equations. Specifically, the detail factors for Föster energy transfer rate, the enhancement of local optical power density, and pump power absorption are studied to reveal the effects of Ba<sup>2+</sup> dopant. To be noted, the main effect of Ba<sup>2+</sup> is to modulate the site occupation and ionic environment of the lanthanide ions. However, the subtle site variation of lanthanide ions could hardly be distinguished by conventional measurements (UV–Vis and Raman measurements, for example). Clearly, a more in-depth insight into the site occupation of lanthanide could help to investigate UC mechanism and promote UC efficiency. On the other hand, since the UC intensity changes with ion distance, we deduce the dynamic process of the UC luminescence changes at different site occupations of lanthanide ions. Thus, the concentration of Ba<sup>2+</sup> are carried out from 0 to 9 mol% to cover all types of occupation cases in Li-vacancy model to reveal the connection between site occupation and UC spectra systematically, which could modulate the distance between lanthanide ions and promote the ET rate as well.

## 2. Experiment

High purity (99.99%) lithium carbonate (Li<sub>2</sub>CO<sub>3</sub>), niobium oxide (Nb<sub>2</sub>O<sub>5</sub>), barium carbonate (BaCO<sub>3</sub>), thulium oxide (Tm<sub>2</sub>O<sub>3</sub>), and ytterbium oxide (Yb<sub>2</sub>O<sub>3</sub>) are used for the synthesis of doped congruent LiNbO<sub>3</sub> polycrystal. The raw mixture is grinded in mortar for 2 h to guarantee the uniformity. Then, the CLN (molar ratio [Li]/[Nb] = 0.946) polycrystal is synthesized via high temperature solid-phase method which is annealed at 1150 °C for 5 h to guarantee sufficient reaction. The doped samples of 0.5 Tm<sup>3+</sup>/2 Yb<sup>3+</sup>/0, 1, 3, 5, 7, 9 mol% Ba<sup>2+</sup>:LN (samples #1–6) are synthesized by the same process.

The purity and phase structure of the production are measured using a Bruker D8 ADVANCE X-ray power diffraction (XRD) via Cu K $\alpha$  radiation diffractometer ( $\lambda = 1.54 \text{ \AA}$ ) in a  $2\theta$  range from 20° to 70°. UV–VIS–NIR spectrophotometer (UV-3600, SHIMADZU) is used to record UV–VIS absorption spectra. Raman spectra are recorded with a Renishaw inVia under excitation wavelength of 785 nm in a scan range from 100 to 3200 cm<sup>-1</sup>. Photoluminescence spectra are recorded with an Edinburgh FLSP920 under 980 nm laser excitation. The UC spectra-based steady state rate equations are listed to investigate the main factors that affect UC process.

## 3. Results

The purity and phase structure of samples are characterized by XRD measurement. As shown in Fig. 1(a), all diffraction peaks of 0–9 mol% Ba<sup>2+</sup> doped Tm<sup>3+</sup>/Yb<sup>3+</sup>:LN match well with the standard PDF card #82–2409. The extra peaks at 26.5° and 28.1° appearing in samples #5 and #6 could be attributed to the excess dopant. To further investigate the lattice structure, as shown in Fig. 1(b and c), UV–Vis and Raman measurements are taken to study the site occupation of Ba<sup>2+</sup> dopants in LN polycrystal. Specifically, Fig. 1(b) presents the UV–Vis spectra of Tm<sup>3+</sup>/Yb<sup>3+</sup>:LN with different Ba<sup>2+</sup> concentrations, the UV absorption edge shows a strong dependence on Ba<sup>2+</sup> concentration. The Raman spectra ranging from 100 to 3200 cm<sup>-1</sup> are demonstrated in Fig. 1(c). The vibration at 150 cm<sup>-1</sup> attributes to the Li<sup>+</sup> ion translational vibration, assigning to the E(TO1) vibration [33]. Moreover, A1(TO1) and A1(TO2) modes are sensitive to the changes of Nb and Li motions centered at 250–310 cm<sup>-1</sup> [34]. The frequencies of A1(TO1) and A1(TO2) modes

based on Ba<sup>2+</sup> concentrations are shown in Fig. 1(d).

The UC spectra of Tm<sup>3+</sup>/Yb<sup>3+</sup>:LN with different Ba<sup>2+</sup> concentrations are obtained under excitation of 980 nm diode laser. As shown in Fig. 2, we point out the UC intensity increases in 1 mol% Ba<sup>2+</sup> sample and decreases inversely with doping concentration until 5 mol%, then increases to the maximum value in 9 mol% Ba<sup>2+</sup> sample. This doping-based UC variation can be divided into three stages: descent stage (stage I, 1–3 mol% Ba<sup>2+</sup>), turning stage (stage II, 3–5 mol% Ba<sup>2+</sup>) and ascent stage (stage III, 5–9 mol% Ba<sup>2+</sup>).

Among all UC spectra, the main peak of blue light centered at 468 nm attributes to the Tm<sup>3+</sup>:  $^1G_4 \rightarrow ^3H_6$  transition, the peaks of red light centered at 644 nm attribute to the transition of Tm<sup>3+</sup>:  $^1G_4 \rightarrow ^4I_{13/2}$ . Notably, the intensity of visible blue and red emission demonstrates that Ba<sup>2+</sup> ions could enhance the fluorescence signal by 4.8 and 7.9 times, respectively. To study this UC mechanism further, the UC spectra are measured under different pump powers. Fig. 3 presents the dependence of UC emission intensity on pump power (from 300 to 950 mW). Specifically, as shown in Fig. 3(a), the luminescence intensity exhibits cubed and quadratic dependence on the excitation power density under weak and strong excitation regions, respectively. The ordinate refers to the integrated intensity of corresponding emission band. The enhancement factors are demonstrated in Fig. 3(b), transforming from 4.8 to 0.7 with the increasing pump power.

## 4. Discussion

**Raman and UV–Vis spectra analysis.** Combining the three doping stages (I, II and III) in the UC, UV and Raman spectra of the tri-doping system, the specific site occupation process of lanthanide ion could be presented vividly, which becomes a clear clue to further reveal the mechanism of the enhanced emission. In stage I (1–3 mol% Ba<sup>2+</sup>), the red shift of UV absorption edge occurs and the peak position of E(TO1) vibration remains unchanged. Specifically, the peak intensity of E(TO1) increases for the valence compensation in 1 mol% Ba<sup>2+</sup> sample and then decreases inversely with doping concentration, indicating Ba<sup>2+</sup> replaces Nb<sub>Li</sub><sup>4+</sup> antisite primarily, and then takes Li sites [35]. Additionally, the frequencies of A1(TO1) and A1(TO2) modes diminish, indicating the dopant start to take Nb site [36]. In stage II (3–5 mol% Ba<sup>2+</sup>) the blue shift of UV absorption edge occurs, meanwhile, the peak position of E(TO1) vibration shifts to the higher frequency region, indicating the reinforcement of Li–O bond. The frequencies of A1(TO1) and A1(TO2) modes increase as well, suggesting Ba<sup>2+</sup> replaces Nb<sup>5+</sup> site in this stage. Then, in stage III (7–9 mol%), the UV absorption edge slightly shifts with increasing Ba<sup>2+</sup>. The peak position of E(TO1) vibration shifts to the higher frequency region while the intensity decreases. Meanwhile, frequencies of A1(TO1) and A1(TO2) modes decrease in 7 mol% Ba<sup>2+</sup> sample and shift in a small margin in 9 mol% Ba<sup>2+</sup> sample. Thus, in this stage, Ba<sup>2+</sup> takes Li and Nb sites simultaneously and the former one dominates. However, as the core issue of phosphor, the complex site occupation of multiple lanthanide and UC mechanism in each doping stage are still unexplained.

**Mechanism of UC enhancement.** Based on the sensitive 4f levels, UC spectra could offer considerable evidence to reveal the ET process. Especially the factors for Föster ET rate, local optical power density and pump power absorption could be taken into consideration for further investigation. The ET rate can be quantified by steady state rate equations to visualize the site occupation process of lanthanide ions. Fig. 4(a) illustrates the ET process of blue and red emission. The energy from an excited Yb<sup>3+</sup> can promote Tm<sup>3+</sup> from ground state to  $^3H_5$  state ( $^3H_6 \rightarrow ^3H_5$  transition, ET1). The intermediate state level  $^3H_5$  could relaxes to  $^3F_4$  state via non-radiation relaxation ( $^3H_5 \rightarrow ^3F_4$ ). Then, the  $^3F_4$  state can be excited via ET2 to the  $^3F_2$ ,  $^3F_3$  states ( $^3F_4 \rightarrow ^3F_2$ ,  $^3F_3$  transition, ET2). Right after that,

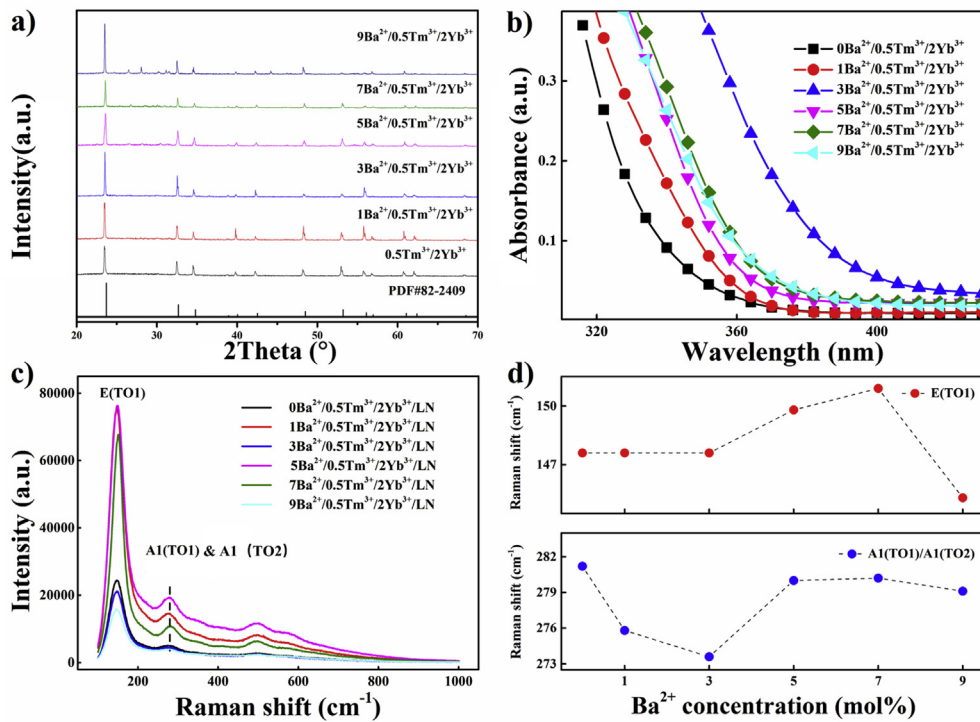


**Fig. 1.** Structure characterization of  $\text{Tm}^{3+}/\text{Yb}^{3+}:\text{LN}$  in different  $\text{Ba}^{2+}$  concentrations: (a) X-ray diffraction patterns, (b) ultraviolet–vis absorption spectra, (c) and Raman spectra. (d) The Raman shift of E(TO1) and A1(TO1)/A1(TO2) modes.

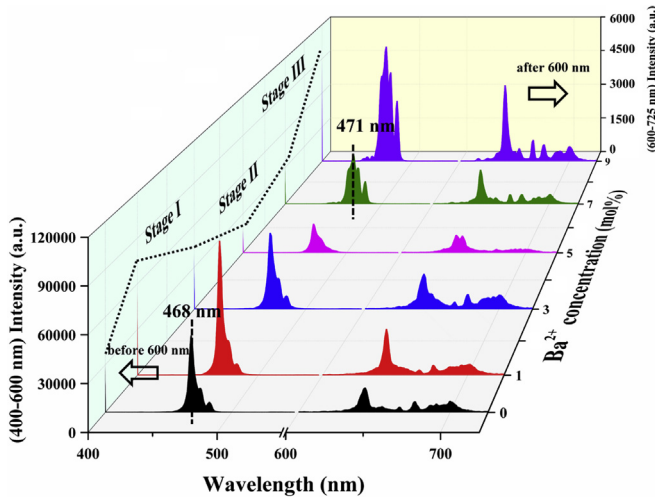


**Fig. 2.** The UC emission variation of  $\text{Tm}^{3+}/\text{Yb}^{3+}:\text{LN}$  with different  $\text{Ba}^{2+}$  ion concentrations under pump power of 0.5 W.

$^3\text{F}_2$  and  $^3\text{F}_3$  relax to  $^3\text{H}_4$  state via non-radiation relaxation ( $^3\text{F}_2 \rightarrow ^3\text{H}_4$ ). Subsequently, the  $\text{Tm}^{3+}$  ions at  $^3\text{H}_4$  can be further excited to  $^1\text{G}_4$  state via ET3 ( $^3\text{H}_4 \rightarrow ^1\text{G}_4$  transition, ET3), after which UC blue and red emission can be achieved. Since the UC blue signal is much stronger than the red one in all samples, the following discussion focuses on the UC blue luminescence.

To reveal the effect of  $\text{Ba}^{2+}$ , the enhancement factors of blue and red emission are presented in Fig. 3(b). We can point out that the enhancement factor varies rapidly at different excitation power ranging in 300–500 mW, and then, approaches to a constant value at higher power density. Due to the dominate ET process, the enhancement factor at high power density can be regarded as the

enhancement of 980 nm absorption. The enhancement factor approaches to 0.7 in 9 mol%  $\text{Ba}^{2+}$  sample, indicating  $\text{Ba}^{2+}$  dopant is detrimental for 980 nm photon harvest [37].

**Steady state rate equation.** Based on the analyzed ET process between  $\text{Tm}^{3+}$  and  $\text{Yb}^{3+}$ , the steady-state rate equations could quantify the ET rate in Equations (1)–(7) [1,38,39].

$$\frac{dN_{S1}}{dt} = 0 = \sigma\Phi N_{S0} - W_{S10}N_{S1}N_{L0} - R_{ET1}N_{S1}N_{L0} - R_{ET2}N_{S1}N_{L1} - R_{ET3}N_{S1}N_{L2} \quad (1)$$

$$\frac{dN_{L1}}{dt} = 0 = R_{ET1}N_{S1}N_{L0} - W_{L10}N_{L1} - R_{ET2}N_{S1}N_{L1} + W_{L41}N_{L4} \quad (2)$$

$$\frac{dN_{L2}}{dt} = 0 = W_{L32}N_{L3} - R_{ET3}N_{S1}N_{L2} - W_{L20}N_{L2} \quad (3)$$

$$\frac{dN_{L3}}{dt} = 0 = R_{ET2}N_{S1}N_{L1} - W_{L32}N_{L3} - W_{L30}N_{L3} \quad (4)$$

$$\frac{dN_{L4}}{dt} = 0 = R_{ET3}N_{S1}N_{L2} - W_{L40}N_{L4} - W_{L41}N_{L4} \quad (5)$$

$$N_L = N_{L0} + N_{L1} + N_{L2} + N_{L3} + N_{L4} \quad (6)$$

$$N_S = N_{S0} + N_{S1} \quad (7)$$

where  $N_{Li}$  is the density of the energy state  $i$  of  $\text{Tm}^{3+}$ .  $N_{S0}$  and  $N_{S1}$  represent the  $^2\text{F}_{5/2}$  and  $^2\text{F}_{7/2}$  levels of the sensitizer  $\text{Yb}^{3+}$ , respectively.  $\sigma$  is the absorption cross section of 980 nm and  $\Phi$  is the incident light flux.  $W$  is the decay rate with a subscript representing

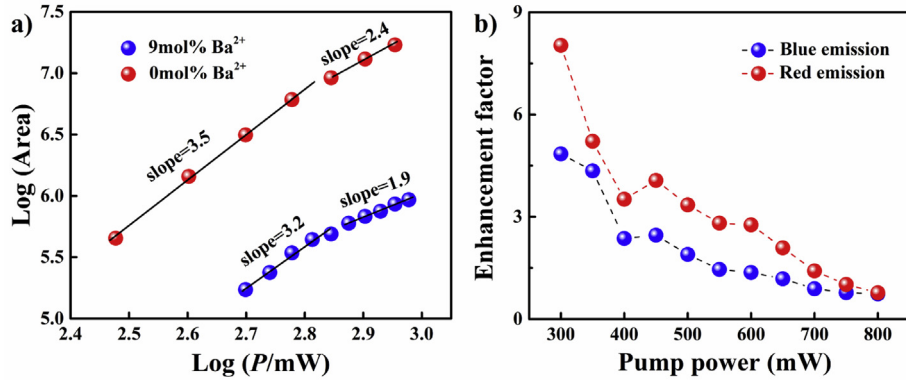


**Fig. 3.** (a) The dependence of blue emission intensity on the pump power in weak and strong excitation region in 0 and 9 mol% Ba<sup>2+</sup> samples, (b) The dependence of the enhancement factors in 9 mol% Ba<sup>2+</sup> sample on different pump power. (For interpretation of the references to colour in this figure legend, the reader is referred to the Web version of this article.)

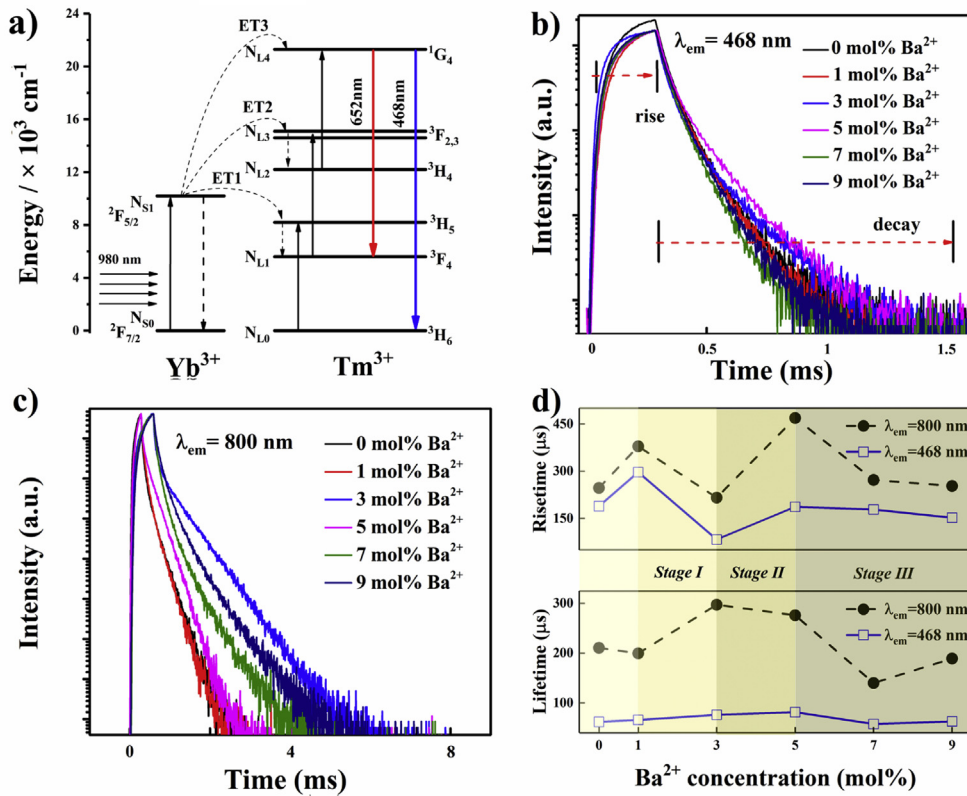


**Fig. 4.** (a) Upconversion mechanism of blue and red emissions of Ba<sup>2+</sup>/Tm<sup>3+</sup>/Yb<sup>3+</sup>:LN polycrystal, (b) The decay curve of 468 nm emission of Tm<sup>3+</sup>/Yb<sup>3+</sup>:LN in different Ba<sup>2+</sup> concentration samples, (c) The decay curve of 800 nm emission of Tm<sup>3+</sup>/Yb<sup>3+</sup>:LN in different Ba<sup>2+</sup> concentration samples, (d) The dependence of lifetime and rise time upon Ba<sup>2+</sup> concentration with 468 and 800 nm. (For interpretation of the references to colour in this figure legend, the reader is referred to the Web version of this article.)

the initial and final states of decay process. For instance,  $W_{S10}$  represents the decay rate from S<sub>1</sub>(<sup>2</sup>F<sub>5/2</sub>) to S<sub>0</sub>(<sup>2</sup>F<sub>7/2</sub>) state of Yb<sup>3+</sup> ion.  $R_{ET1}$ ,  $R_{ET2}$  and  $R_{ET3}$  are the energy transfer coefficients for the Förster energy transfer processes between the donor and the acceptor in ET1, 2 and 3 process, respectively. Then,  $N_S$  and  $N_L$  represents the densities of donor and acceptor, respectively. In addition, the  $W_{L30}N_{L3}$  and  $W_{L41}N_{L4}$  can be neglected for the weak signal in fluorescence spectra.

The decay process is dominant in the weak excitation region, therefore, the  $R_{ET1,2,3}N_{S1}N_{L0,1,2}$  in Equation (1) and  $R_{ET2}N_{S1}N_{L1}$  in Equation (2) can be neglected to simplify the expressions. Combining Equations (1)–(5), the expression of the blue UC

fluorescence intensity in weak excitation limit could be given:

$$\Phi_{Blue}^{weak} = \frac{R_{ET1}R_{ET2}R_{ET3}N_L N_S^3}{W_{L10}W_{S10}^3(R_{ET3}N_S + W_{L20})} \cdot (\sigma\Phi)^3 \quad (8)$$

where the blue UC fluorescence signal shows cubic dependence on the incident photon flux, which is highly consistent with the experimental data in Fig. 3(a). The energy transfer process is dominate in strong excitation region, so the decay process in Equation (1) and Equation (2) can be neglected. Thus, the expression of the blue UC fluorescence intensity in strong excitation limit

could be drawn:

$$\Phi_{Blue}^{strong} = \frac{R_{ET3}N_{SO}^2(R_{ET1}N_{L0} - R_{ET3}N_{L2})}{W_{L20} \cdot (2R_{ET1}N_{L0} + R_{ET3}N_{L2})^2} \cdot (\sigma\Phi)^2 \quad (9)$$

where the blue UC fluorescence signal shows quadratic dependence on the incident photon flux, which is consistent with the experimental data in Fig. 3(a) in both weak and strong excitation regions. The transition between the week and strong excitation occurs at the same excitation pump power, indicating no enhancement of local optical power density after  $\text{Ba}^{2+}$  doping. The enhancement factor could be simplified as Equations (10) and (11):

$$F_{weak} = \frac{F_{ET1}F_{ET2}F_\alpha^2}{F_{ET3}F_p^n} \quad (10)$$

$$F_{strong} = F_\alpha \quad (11)$$

where  $F_{ET1}$ ,  $F_{ET2}$ , and  $F_{ET3}$  are the enhancement factors for the ET processes correlated with coefficients of  $R_{ET1}$ ,  $R_{ET2}$  and  $R_{ET3}$ , respectively;  $F_\alpha$  is the absorption enhancement factor;  $F_p$  is the Purcell factor, corresponding to the enhancement factor of the radiative decay rate.  $n$  is either 0 or 3, which depends on the dominant channel of the donor decay [3]. Here,  $n$  equals to 0 in 9 mol%  $\text{Ba}^{2+}$  sample. For the strong excitation region, the energy transfer process dominates the field enhancement factor caused by  $\text{Ba}^{2+}$  doping. As shown in Fig. 3(b), the enhancement factor is 0.7 under 800 mW, indicating that  $\text{Ba}^{2+}$  doping decreases the absorption of pump laser. The  $F_{weak}$  equal to 4.8 in 9 mol %  $\text{Ba}^{2+}$  sample, which implies  $F_{ET1}F_{ET2}/F_{ET3} = 9.8$ . The electronic populated at  ${}^3\text{H}_4$  state can be excited to  ${}^1\text{G}_4$  state or decay to the ground state. Thus,  $F_{ET3}$  can be obtained by Equation (12):

$$F_{ET3} = \frac{I_{9\text{mol}\%}}{I_{0\text{mol}\%}} \quad (12)$$

$$I_{0\text{mol}\%} = \frac{I_{0\text{mol}\%}^{468}}{I_{0\text{mol}\%}^{468} + I_{0\text{mol}\%}^{800}} \quad (13)$$

$$I_{9\text{mol}\%} = \frac{I_{9\text{mol}\%}^{471}}{I_{9\text{mol}\%}^{471} + I_{9\text{mol}\%}^{800}} \quad (14)$$

$I_{X\text{mol}\%}^Y$  is integration of the peak centered at  $Y$  nm in  $X$  mol%  $\text{Ba}^{2+}$  doped sample. Then,  $F_{ET3}$  should be 1.8, and  $F_{ET1} \times F_{ET2}$  equals to 17.6. Based on the occupation analyzation, the UC enhancement could be revealed by the ion distance of Tm–Yb pairs in different  $\text{Ba}^{2+}$  doping stages. Specifically, four types of Tm–Yb pairs could be listed in an ascending order of ion distance ( $\text{Tm}_{\text{i}}^{3+} - \text{Yb}_{\text{Nb}}^{2-} < \text{Tm}_{\text{Li}}^{2+} - \text{Yb}_{\text{Nb}}^{2-} < \text{Tm}_{\text{Li}}^{2+} - \text{Yb}_{\text{Li}}^{2+} = \text{Tm}_{\text{Nb}}^{2-} - \text{Yb}_{\text{Nb}}^{2-}$ , sites of  $\text{Tm}^{3+}$  and  $\text{Yb}^{3+}$  ions are interchangeable and subscripts i represents interstitial void), accordingly, the mechanism of UC enhancement could be revealed as follow. In stage I, at the beginning,  $\text{Tm}_{\text{Li}}^{2+} - \text{Yb}_{\text{Li}}^{2+}$  pairs are the majority in  $\text{Ba}^{2+}$ -free sample. Then, as the  $\text{Ba}^{2+}$  doping concentration increases to 1 mol%,  $\text{Ba}^{2+}$  takes  $\text{Nb}_{\text{Li}}^{4+}$  site to decrease the symmetry of local crystal field, giving rise to an enhanced UC luminescence in 1 mol%  $\text{Ba}^{2+}$  sample. After that,  $\text{Ba}^{2+}$  takes Li site and lanthanide ions are pushed to Nb sites to form  $\text{Tm}_{\text{Nb}}^{2-} - \text{Yb}_{\text{Li}}^{2+}$  pairs. Due to the less affected environment around Nb site by  $\text{Ba}^{2+}$  dopant, the optical active ion  $\text{Tm}^{3+}$  at Nb is disadvantage to radiate with higher local crystal field symmetry, and therefore, the UC intensity decreases. In stage II, the UC intensity reaches the lowest value, attributing to the saturation of  $\text{Tm}_{\text{Nb}}^{2-} - \text{Yb}_{\text{Li}}^{2+}$  pairs. In stage III, since the extra  $\text{Ba}^{2+}$  turns to occupy Nb site, pushing lanthanide

ions to the interstitial void ( $\text{Tm}_{\text{i}}^{3+} - \text{Yb}_{\text{Nb}}^{2-}$ ), which explains the extra peaks appearing in heavy doped samples. Moreover, a closer distance between  $\text{Ba}^{2+}$  and lanthanide ions is detrimental to the symmetry of local crystal field, therefore, increasing the 4f-4f transition possibility. Notably, the changed site occupation of lanthanide ions is reflected on the UC peak position. If we look closely at Fig. 2, a distinct variation that the emission peak centered at 468 nm shifts to 471 nm when  $\text{Ba}^{2+}$  concentration reaches 5 mol % could be seen, which arises from the nephelauxetic effect. The nephelauxetic effect depends on the covalency of chemical bond to luminescence center. The red shift implies a great variation of electronic cloud density between  $\text{O}^{2-}$  and  $\text{Tm}^{3+}$  (caused by  $\text{Ba}^{2+}$  dopant), which verifies the site migration. Theoretical analyzation affirms that the UC enhancement is attributed to the promoted ET rate which is mainly manipulated by different site occupation. To further verify the analysis result, time-resolved measurement is used to characterize the dynamic process of the emission level.

**The decay curve of luminescence.** The time-resolved measurement could present the dynamic process of 4f states. Fig. 4(b) and (c) show the decay curves of 468 nm and 800 nm emission of  $\text{Tm}^{3+}/\text{Yb}^{3+}:\text{LN}$  in different concentration of  $\text{Ba}^{2+}$ , respectively. The fluorescence dynamic curves of 468 nm ( ${}^1\text{G}_4 \rightarrow {}^3\text{H}_6$ ) and 800 nm ( ${}^3\text{H}_4 \rightarrow {}^3\text{H}_6$ ) of  $\text{Tm}^{3+}$  in LN for different  $\text{Ba}^{2+}$  concentrations are measured under 980 nm laser excitation and the risetime and lifetime results are drawn in Fig. 4(d). The single exponential and double exponential functions are applied to match the rising curve and decay curve, respectively. As shown in Equations (15) and (16):

$$I(t) = I_a + Ae^{-\frac{t}{\tau}} \quad (15)$$

$$I(t) = I_b + Ae^{\frac{-t}{\tau_s}} + Ae^{\frac{-t}{\tau_f}} \quad (16)$$

An intense variation is observed for the lifetime of 800 nm emission compared to 468 nm lifetime. According to Equation (8), the lifetime of 800 nm positively relates to the luminescence intensity. However, in our case, the lifetime of 800 nm emission variates against the UC intensity, indicating the ET process dominates the UC process in this system. Due to the distance dependent RT rate, the risetime could draw the  $\text{Tm}^{3+}-\text{Yb}^{3+}$  distance, which is consistent with the site occupation analyzation. To have a better understanding of the entire procedure, all the derivative processes are listed orderly in Table 1.

The UV–Vis and Raman spectra are used to investigate the site occupation of  $\text{Ba}^{2+}$ . Then, based on the UC spectra, the theory analyzation reveals the UC mechanism. Afterwards, the site occupation of lanthanide ions can be deduced. Moreover, the time resolved measurement, regarded as the corroborative evidence of ET variation, presents the variation of the kinetic process of  ${}^1\text{G}_4$  and  ${}^3\text{H}_4$  states. Our study presents the detail of the variation of UC intensity with  $\text{Ba}^{2+}$  doping by demonstrating the different lanthanide site occupation, which serves to design the phosphor structure for better performance.

## 5. Conclusions

The  $\text{Tm}^{3+}/\text{Yb}^{3+}:\text{LN}$  in 0, 1, 3, 5, 7, 9 mol%  $\text{Ba}^{2+}$  tri-doping samples have been synthesized, and the UC blue and red emission are enhanced by 4.8 and 7.9 folds, respectively. The steady-state rate equations point out a three-photons process is involved to generate the blue UC emission under weak power density. However, under the strong power density, the emission turns to a two-photons process. The UC intensity presents zigzag-shaped variation, which attributes to the different site occupation of  $\text{Ba}^{2+}$  ion. Since the changed symmetry of local crystal field,  $\text{Ba}^{2+}$  could tailor the UC

**Table 1**  
Results from each measurement.

Measurement	Stage I	Stage II	Stage III
UV	$\text{Nb}_{\text{Li}}^{4+} \& \text{Li}_{\text{Li}} \rightarrow \text{Ba}_{\text{Li}}^{+}$	$\text{Nb}_{\text{Nb}} \rightarrow \text{Ba}_{\text{Nb}}^{3-}$	$\text{Li}_{\text{Li}} \rightarrow \text{Ba}_{\text{Li}}^{+} \& \text{Nb}_{\text{Nb}} \rightarrow \text{Ba}_{\text{Nb}}^{3-}$
Raman	$\text{Li}_{\text{Li}} \rightarrow \text{Ba}_{\text{Li}}^{+}$	$\text{Nb}_{\text{Nb}} \rightarrow \text{Ba}_{\text{Nb}}^{3-}$	$\text{Li}_{\text{Li}} \rightarrow \text{Ba}_{\text{Li}}^{+}$
Enhancement factor <sup>a</sup>	1.83 → 1.12	1.12 → 0.46	0.46 → 2.08
SSR Eqs. <sup>b</sup>	$\text{Tm}_{\text{Li}}^{2+} - \text{Yb}_{\text{Nb}}^{2-}, \text{Tm}_{\text{Nb}}^{2-} - \text{Yb}_{\text{Nb}}^{2-}$	$\text{Tm}_{\text{Nb}}^{2-} - \text{Yb}_{\text{Nb}}^{2-}$	$\text{Tm}^{3+} - \text{Yb}_{\text{Nb}}^{2-}$ <sup>c</sup>
Rise time ( $\mu\text{s}$ ) <sup>d</sup>	297 → 83	83 → 187	187 → 152

<sup>a</sup> Excitation power 0.5 W.

<sup>b</sup> Steady-state rate equations.

<sup>c</sup> Subscript i represents interstitial void, sites of  $\text{Tm}^{3+}$  and  $\text{Yb}^{3+}$  ions are interchangeable.

<sup>d</sup> The rise time is a corroborative evidence of ET rate variation.

intensity by different crystal site. Therefore, the UC spectra illustrate an approach to visualize the specific dynamic process of lanthanide ion occupation in crystal lattice. Meanwhile, the time-resolved fluorescence measurement proves the enhanced ET process can be achieved with specific concentration due to the different site occupation. This study achieves an efficient feedback of the lanthanides movement through UC spectra and promotes UC efficiency by modulating site occupation purposefully.

## Declaration of competing interest

The authors declare that they have no known competing financial interests or personal relationships that could have appeared to influence the work reported in this paper.

## CRediT authorship contribution statement

**Zhihua Liu:** Investigation, Data curation, Writing - original draft. **Yunzhong Zhu:** Conceptualization, Validation, Writing - review & editing. **Wenjia Wang:** Investigation, Software. **Decai Ma:** Project administration. **Biao Wang:** Supervision, Funding acquisition.

## Acknowledgment

This work was supported by the National Natural Science Foundation of China (NSFC) (51802358; 11832019); National Natural Science Foundation of Guangdong, China (2018A030313321; 2017A0303104 26); Science and Technology Program of Guangzhou, China (201904010246).

## Appendix A. Supplementary data

Supplementary data to this article can be found online at <https://doi.org/10.1016/j.jallcom.2020.153990>.

## References

- G. Chen, H. Ågren, T.Y. Ohulchansky, P.N. Prasad, Light upconverting core-shell nanostructures: nanophotonic control for emerging applications, *Chem. Soc. Rev.* 44 (2015) 1680–1713.
- J. Komar, R. Lisiecki, R. Kowalski, B. Macalik, P. Solarz, M. Glowacki, M. Berkowski, W. Ryba-Romanowski, Down- and upconversion phenomena in  $\text{Gd}_3[\text{Al},\text{Ga}]_5\text{O}_12$  crystals doped with  $\text{Pr}^{3+}$  and  $\text{Yb}^{3+}$  ions, *J. Phys. Chem. C* 122 (2018) 13061–13071.
- A. Shalav, B.S. Richards, T. Trupke, K.W. Kramer, H.U. Gudel, Application of  $\text{NaYF}_4:\text{Er}^{3+}$  up-converting phosphors for enhanced near-infrared silicon solar cell response, *Appl. Phys. Lett.* 86 (2005), 013505.
- J. Zhang, G.B. Chen, Z.Y. Zhai, H.B. Chen, Y.M. Zhang, Optical temperature sensing using upconversion luminescence in rare-earth ions doped  $\text{Ca}_2\text{Gd}_8(\text{-SiO}_4)_6\text{O}_2$  phosphors, *J. Alloys Compd.* 771 (2019) 838–846.
- G. Chen, H. Qiu, P.N. Prasad, X. Chen, Upconversion nanoparticles: design, nanochemistry, and applications in theranostics, *Chem. Rev.* 114 (2014) 5161–5214.
- G. Leménager, M. Thiriet, F. Pourcin, K. Lahli, F. Valdivia-Valero, G. Colas des Francs, T. Gacoin, J. Fick, Size-dependent trapping behavior and optical emission study of  $\text{NaYF}_4$  nanorods in optical fiber tip tweezers, *Optic Express* 26 (2018) 32156–32167.
- Y. Tian, Y. Tian, P. Huang, L. Wang, Q. Shi, C. Cui, Effect of  $\text{Yb}^{3+}$  concentration on upconversion luminescence and temperature sensing behavior in  $\text{Yb}^{3+}/\text{Er}^{3+}$ , co-doped  $\text{YNbO}_4$ , nanoparticles prepared via molten salt route, *Chem. Eng. J.* 297 (2016) 26–34.
- J. Xu, D. Yang, W. Han, S. Dong, T. Jia, F. He, H. Bi, S. Gai, L. Li, P. Yang, A novel strategy for markedly enhancing the red upconversion emission in  $\text{Er}^{3+}/\text{Tm}^{3+}$  cooperated nanoparticles, *J. Mater. Chem. C* 6 (2018) 7533.
- N. Zhang, M.S. Molokeev, Q. Liu, Z. Xia, Pure red upconversion luminescence and optical thermometry of  $\text{Er}^{3+}$  doped sensitizer-rich  $\text{SrYbInO}_4$  phosphors, *J. Mater. Chem. C* 6 (2018) 7361.
- J. Milliez, A. Rapaport, M. Bass, A. Cassanho, H.P. Jenssen, High-brightness white-light source based on up-conversion phosphors, *J. Disp. Technol.* 2 (2006) 307–311.
- E. Downing, L. Hesselink, J. Ralston, R. Macfarlane, A three-color, solid-state, three-dimensional display, *Science* 273 (1996) 1185–1189.
- D. Lu, S.K. Cho, S. Ahn, L. Brun, C.J. Summers, W. Park, Plasmon enhancement mechanism for the upconversion processes in  $\text{NaYF}_4:\text{Yb}^{3+},\text{Er}^{3+}$  nanoparticles: maxwell versus Förster, *ACS Nano* 8 (2014) 7780–7792.
- L. Dai, C.R. Liu, X.B. Han, L.P. Wang, Y. Shao, Y.H. Xu, Effect of  $\text{Ho}^{3+}$  and  $\text{Tm}^{3+}$  concentration on UV-VIS-NIR and upconversion luminescence in  $\text{Ho}:\text{Tm}:\text{LiNbO}_3$  crystals, *J. Alloys Compd.* 771 (2019) 960–963.
- G. Chen, H. Liu, H. Liang, S. Gabriel, Z. Zhang, Upconversion emission enhancement in  $\text{Yb}^{3+}/\text{Er}^{3+}$ -codoped  $\text{Y}_2\text{O}_3$  nanocrystals by tridoping with  $\text{Li}^+$  ions, *J. Phys. Chem. C* 112 (2008) 12030–12036.
- M.Y. Hossain, Amy Hor, Q.A. Luu, S.J. Smith, P.S. May, M.T. Berry, Explaining the nanoscale effect in the upconversion dynamics of  $\beta\text{-NaYF}_4:\text{Yb}^{3+},\text{Er}^{3+}$  core and Core–Shell nanocrystals, *J. Phys. Chem. C* 121 (2017) 16592–16606.
- A. Dubey, A.K. Soni, A. Kumar, R. Dey, V.K. Rai, Enhanced green upconversion emission in  $\text{NaYF}_4:\text{Er}^{3+}/\text{Yb}^{3+}/\text{Li}^+$  phosphors for optical thermometry, *J. Alloys Compd.* 693 (2017) 194–200.
- H. Zhang, Y. Li, I.A. Ivanov, Y. Qu, Y. Huang, X. Duan, Plasmonic modulation of the upconversion fluorescence in  $\text{NaYF}_4:\text{Yb/Tm}$  hexaplate nanocrystals using gold nanoparticles or nanoshells, *Angew. Chem. Int. Ed.* 49 (2010) 2865–2868.
- T. Cong, Y. Ding, J. Liu, H. Zhao, X. Hong, Synthesis and optical properties of  $\text{Zn}^{2+}$ , doped  $\text{NaYF}_4:\text{Yb}^{3+},\text{Er}^{3+}$ , upconversion nanoparticles, *Mater. Lett.* 165 (2016) 59–62.
- M. Wu, X.F. Jiang, E.H. Song, J. Su, Z.T. Chen, W.B. Dai, S. Ye, Q.Y. Zhang, Tailoring the upconversion of  $\text{ABF}_3:\text{Yb}^{3+}/\text{Er}^{3+}$  through  $\text{Mn}^{2+}$  doping, *J. Mater. Chem. C* 4 (2016) 9598–9607.
- K.L. Reddy, V. Srivinas, K.R. Shankar, S. Kumar, V. Sharma, A. Kumar, A. Bahuguna, K. Bhattacharyya, V. Krishnan, Enhancement of luminescence intensity in red emitting  $\text{NaYF}_4:\text{Yb/Ho/Mn}$  upconversion nanophosphors by variation of reaction parameters, *J. Phys. Chem. C* 121 (2017) 11783–11793.
- D. Chen, W. Xu, S. Yuan, X. Li, J. Zhong,  $\text{Ln}^{3+}$ -Sensitized  $\text{Mn}^{4+}$  near-infrared upconverting luminescence and dual-modal temperature sensing, *J. Mater. Chem. C* 5 (2017) 9619.
- L. Xing, Y. Xu, R. Wang, W. Xu, Influence of temperature on upconversion multicolor luminescence in  $\text{Ho}^{3+}/\text{Yb}^{3+}/\text{Tm}^{3+}$ -doped  $\text{LiNbO}_3$  single crystal, *Opt. Lett.* 38 (2013) 2535–2537.
- Y.Z. Zhu, S.P. Lin, Y. Zheng, D.C. Ma, B. Wang, Improvement of pyroelectric figures of merit in zirconia-doped congruent lithium niobate single crystals, *J. Mater. Sci.* 51 (2016) 3155–3161.
- L. Arizmendi, Review article: photonic applications of lithium niobate crystals, *Phys. Status Solidi* 201 (2004) 253–283.
- D.L. Zhang, J. Gao, P.R. Hua, D.Y. Yu, E.B. Pun, Appropriate solvent  $\text{NaVO}_3$  for composition analysis of  $\text{LiNbO}_3$  crystal using chemical method, *Anal. Chem.* 85 (2013) 1940–1944.
- S. Long, D. Ma, Y. Zhu, M. Yang, S. Lin, B. Wang, Temperature dependence of white light emission and energy transfer in  $\text{Dy}^{3+}$  and  $\text{Tm}^{3+}$  co-doped  $\text{LiNbO}_3$  single crystals, *J. Lumin.* 192 (2017) 728–733.
- S.P. Lin, C.W. Xiong, D.C. Ma, H.S. Li, S.W. Long, B. Wang, Persistent luminescence found in  $\text{Mg}^{2+}$  and  $\text{Pr}^{3+}$  co-doped  $\text{LiNbO}_3$  single crystal, *J. Mater. Chem. C* 6 (2018) 10067.

- [28] Y. Zhu, S. Lin, Z. Liu, W. Wang, D. Ma, B. Wang, In situ visualization of the quasi-periodic crystal growth interface fluctuation by growth interface electromotive force spectrum in a Czochralski system, *CrystEngComm* 21 (2019) 1107–1113.
- [29] Y. Li, Y. Li, R. Wang, Y. Xu, W. Zheng, Enhancing upconversion luminescence by annealing processes and the high-temperature sensing of ZnO:Yb/Tm nanoparticles, *New J. Chem.* 41 (2017) 7116–7122.
- [30] G. Galleani, S.H. Santagneli, Y. Ledemi, Y. Messaddeq, Ultraviolet upconversion luminescence in a highly transparent triply-doped  $\text{Gd}^{3+}$ – $\text{Tm}^{3+}$ – $\text{Yb}^{3+}$  Fluoride–Phosphate glasses, *J. Phys. Chem. C* 122 (2018) 2275–2284.
- [31] J.J. Mu, W.J. Sun, F. Li, Y. Guan, X.M. Zhou, J. Li, L. Chen, Upconversion luminescent perovskite  $\text{CaTiO}_3:\text{Yb}^{3+}/\text{Er}^{3+}$  nanocubes, *J. Alloys Compd.* 797 (2019) 1002–1006.
- [32] H. Wu, Z. Hao, L. Zhang, X. Zhang, Y. Xiao, G. Pan, H. Wu, Y. Luo, L. Zhang, J. Zhang, Er<sup>3+</sup>/Yb<sup>3+</sup> codoped phosphor  $\text{Ba}_3\text{Y}_4\text{O}_9$  with intense red upconversion emission and optical temperature sensing behavior, *J. Mater. Chem. C* 6 (2018) 3459.
- [33] L.J. Hu, Y.H. Chang, C.S. Chang, Raman and NMR study in MgO-doped  $\text{LiNbO}_3$  crystal, *Mod. Phys. Lett. B* 5 (1991) 789–797.
- [34] M.D. Fontana, P. Bourson, Microstructure and defects probed by Raman spectroscopy in lithium niobate crystals and devices, *Appl. Phys. Rev.* 2 (2015), 040602.
- [35] W. Wang, R. Wang, W. Zhang, L. Xing, Y. Xu, X. Wu, A computer study and photoelectric property analysis of potassium-doped lithium niobate single crystals, *Phys. Chem. Chem. Phys.* 15 (2013) 14347–14356.
- [36] M.R. Tejerina, K. Pereira da Silva, A.R. Goñi, G.A. Torchia, Hydrostatic-pressure dependence of Raman-active optical phonons in Nd:Mg:LiNbO<sub>3</sub>, *Opt. Mater.* 36 (2013) 581–583.
- [37] W. Park, D. Lu, S. Ahn, Plasmon enhancement of luminescence upconversion, *Chem. Soc. Rev.* 44 (2015) 2940–2962.
- [38] Y. Qu, R. Wang, Z. Qiu, Y. Tao, J. Zhou, White-light upconversion emissions and color tunability of  $12\text{CaO}\cdot 7\text{Al}_2\text{O}_3:\text{Ho}^{3+}/\text{Yb}^{3+}/\text{Tm}^{3+}$ , *Opt. Mater. Express* 5 (2015) 1881–1889.
- [39] G. Chen, T.Y. Ohulchanskyy, R. Kumar, H. Ågren, P.N. Prasad, Ultrasmall monodisperse  $\text{NaYF}_4:\text{Yb}^{3+}/\text{Tm}^{3+}$  nanocrystals with enhanced near-infrared to near-infrared upconversion photoluminescence, *ACS Nano* 4 (2010) 3163–3168.